Journal of Materials Chemistry A

ROYAL SOCIETY OF CHEMISTRY

PAPER

View Article Online
View Journal | View Issue

Open Access Article. Published on 05 April 2024. Downloaded on 3/13/2026 3:07:41 PM.
This article is licensed under a Creative Commons Attribution-NonCommercial 3.0 Unported Licence.

Check for updates

Cite this: J. Mater. Chem. A, 2024, 12, 11416

Significant improvement of photocatalytic hydrogen evolution performance in covalent organic frameworks: substituent fine-tuning†

Shaodong Jiang,[ab] Hongyun Niu,[a] Qing Sun,[c] Rusong Zhao,[d] Na Li[d] and Yaqi Cai*[abe]

Received 22nd January 2024
Accepted 3rd April 2024

DOI: 10.1039/d4ta00478g

rsc.li/materials-a

Imine-linked covalent organic frameworks (COFs) have been widely studied in the field of photocatalytic hydrogen production due to their easy synthesis, good crystallinity, tunable pore size and excellent thermal and chemical stability. However, the effect of substituent type on the photocatalytic properties of COFs has been rarely studied. Herein, six COFs with COF-TpPa as the basic skeleton were synthesized by introducing different types of substituents in the *p*-phenylenediamine benzene ring, among which TpPa-CN_2 was prepared for the first time. The COFs showed similar structures but great differences in their photoelectric properties. TpPa-Cl_2 and TpPa-CN_2 demonstrated a superior hydrogen evolution performance compared to the other four COFs when ascorbic acid was used as the electron sacrificial agent and Pt as the cocatalyst. The photocatalytic hydrogen evolution (PHE) rate of TpPa-Cl_2 and TpPa-CN_2 was as high as 99.23 and 76.93 mmol g^{-1} h^{-1}, respectively. The introduction of chlorine and cyanide improved the visible-light response, hydrophilicity and photo-carrier separation ability of TpPa COF, which contributed to the enhanced PHE efficiency of TpPa-Cl_2 and TpPa-CN_2. This study provides a strong basis for the systematic fine-tuning of the structural and physico-chemical properties of COFs aiming to achieve COF materials with ultra-high photocatalytic activity.

1. Introduction

Photocatalytic water decomposition for hydrogen production offers a sustainable solution for obtaining clean energy, thereby addressing the current energy shortage and mitigating environmental pollution. Takata *et al.* discovered that selecting an appropriate cocatalyst to facilitate charge carrier separation between crystal planes in $SrTiO_3$: Al results in an almost 100% apparent quantum efficiency (AEQ) for water decomposition under UV irradiation.[1,2] However, since sunlight contains a significant amount of visible light,[3–5] it becomes imperative to explore visible light-responsive catalysts for water decomposition and hydrogen production. Although semiconductor photocatalysts like titanium dioxide and g-C_3N_4 have displayed high efficiency in photocatalytic hydrogen production,[6–8] their limited ability to absorb visible light poses a significant challenge for practical applications.

Covalent organic frameworks (COFs) are highly crystalline and stable porous polymers composed of light elements such as B, C, and N. They were first reported by the research group of Yaghi in 2005.[9] COFs exhibit various bonding modes, including boroxanes, borates, carbon–nitrogen double bonds (such as amide, hydrazone, and hydrazide), and carbon–carbon double bonds. The carbon–nitrogen double bonds are primarily formed through acid-catalyzed dehydration of aldehydes and amines, and they are known for their high stability, making them the most commonly reported bonding mode in COFs. Due to their high stability, permanent porosity, high specific surface area, large pore size and high carrier mobility, COFs have shown great application prospects in various applications, such as gas storage and separation,[10–12] energy storage,[13,14] catalysis,[15–18] sensing,[19–22] *etc.* COFs also demonstrate great potential in photocatalytic hydrogen evolution due to their high carrier mobility and low electron–hole recombination rate. Additionally, the tunable photo-response and band gap,[23] achieved through the flexible selection of building blocks, make COFs attractive as alternative materials for semiconductor

[a]State Key Laboratory of Environmental Chemistry and Ecotoxicology, Research Center for Eco-Environmental Sciences, Chinese Academy of Sciences, Beijing 100085, China. E-mail: hyniu@rcees.ac.cn

[b]University of Chinese Academy of Sciences, Beijing 100049, China. E-mail: sdjiang_st@rcees.ac.cn

[c]Xiangnan University, NanLing Research Institute for Modern Seed Industry, Chenzhou 423000, China. E-mail: iliky@163.com

[d]Qilu University of Technology (Shandong Academy of Sciences), Shandong Analysis and Test Center, Key Laboratory for Applied Technology of Sophisticated Analytical Instruments of Shandong Province, Jinan 250014, China. E-mail: zhaors1976@126.com; lisac18@126.com

[e]School of Environment, Hangzhou Institute for Advanced Study, University of Chinese Academy of Sciences, Hangzhou 310024, China. E-mail: caiyaqi@rcees.ac.cn

† Electronic supplementary information (ESI) available. See DOI: https://doi.org/10.1039/d4ta00478g

 This journal is © The Royal Society of Chemistry 2024

Open Access Article. Published on 05 April 2024. Downloaded on 3/13/2026 3:07:41 PM.
This article is licensed under a Creative Commons Attribution-NonCommercial 3.0 Unported Licence.

photocatalysts.[24] For instance, Lotsch *et al.* utilized a hydrazone-linked triazine COF as a catalyst for hydrogen gas production, achieving a photocatalytic hydrogen evolution (PHE) rate of up to 1970 μmol h^{-1} g^{-1}.[15] By constructing a COF@g-C_3N_4 heterojunction, Dong *et al.*[25] efficiently produced hydrogen at a PHE rate of 1153 μmol h^{-1} g^{-1}, surpassing the performance of pure COF monomers.[26] Furthermore, the fine adjustment of monomer structures can significantly enhance the PHE activity of COFs.[27–30] Introducing substituents into the COF backbone has been shown to significantly increase the PHE rate. For example, Lotsch *et al.*[2] found that the hydrogen evolution rate of COFs enhanced from 116.58 μmol h^{-1} g^{-1} to 698.68 μmol h^{-1} g^{-1} by the introduction of cyano groups into the ethylene skeleton. Li *et al.* implanted a dicyano group into BD-COF, resulting in a remarkably high PHE rate of the obtained CYANO-COF, 60 850 μmol h^{-1} g^{-1}, which was 30 times larger than that of BD-COF (1975 μmol h^{-1} g^{-1}).[28]

In the past decade, scientists have investigated the factors affecting the photocatalytic performance of semiconductor materials,[31] including the effect of the structure and number of linkers,[32] heteroatom positions,[33] imine bond orientation,[34] carrier separation and complexation,[35] and crystal structure[36] on the photocatalytic performance of covalent organic frameworks (COFs). The substituents in the COF skeleton can effectively adjust the separation of photogenerated electron–hole pairs and their combination, and the substituent effect is recognized as an important factor affecting the catalytic activity of COFs. However, there are few studies on substituent property–activity relationships in the photocatalytic hydrogen evolution (PHE) reaction. In this work, TpPa-1 was used as a basic backbone, and a series of COFs were synthesized using *p*-phenylenediamine (Pa-1) monomers with substituents of different electronic effects (Scheme 1). The performance of these COFs in the PHE reaction was evaluated. The relationship between the COF structure and properties was evaluated by photocurrent (I–T), electrochemical impedance spectroscopy (EIS), X-ray photoelectron spectroscopy (XPS), transmission electron microscopy (TEM), contact angle test (CA) and photocatalytic hydrogen evolution rate measurement. By examining the effects of substituents on COF properties and catalytic performance, this work aims to provide a comprehensive understanding of the structure–property relationships in COFs and shed light on the mechanisms underlying the substituent-induced enhancements in catalytic activity.

2. Results and discussion

Six kinds of COFs with the same skeleton were synthesized by a typical solvothermal method (Table S1†); among them, TpPa-CN_2 was prepared for the first time. The crystalline structure of these six COFs was confirmed through powder X-ray diffraction (PXRD) analysis, as depicted in Fig. 1a. The PXRD patterns exhibited prominent diffraction peaks at $2\theta = 4.5$–$4.7°$ and 25.5°, corresponding to the reflection from the (110) and (001) crystal planes, respectively. To elucidate the structure of these COFs and calculate the unit cell parameter, two possible two-dimensional (2D) models with eclipsed (AA) and staggered stacking (AB) were built using the self-consistent-charge density functional tight-binding (SCC-DFTB) method. As shown in Fig. S1,† the experimental PXRD patterns of TpPa-1, TpPa-Cl_2, TpPa-CN, TpPa-$(CH_3)_2$ and TpPa-CH_3 matched well with the simulated patterns obtained using the eclipsed stacking model and are in good agreement with the PXRD data reported in the literature for AA-stacked TpPa-1. In addition, the experimental PXRD patterns of TpPa-CN_2 matched well with the simulated patterns obtained using the staggered stacking model (Fig. 1a and S1†).

The permanent porosities of COFs were assessed by measuring nitrogen adsorption/desorption isotherms at 77 K.

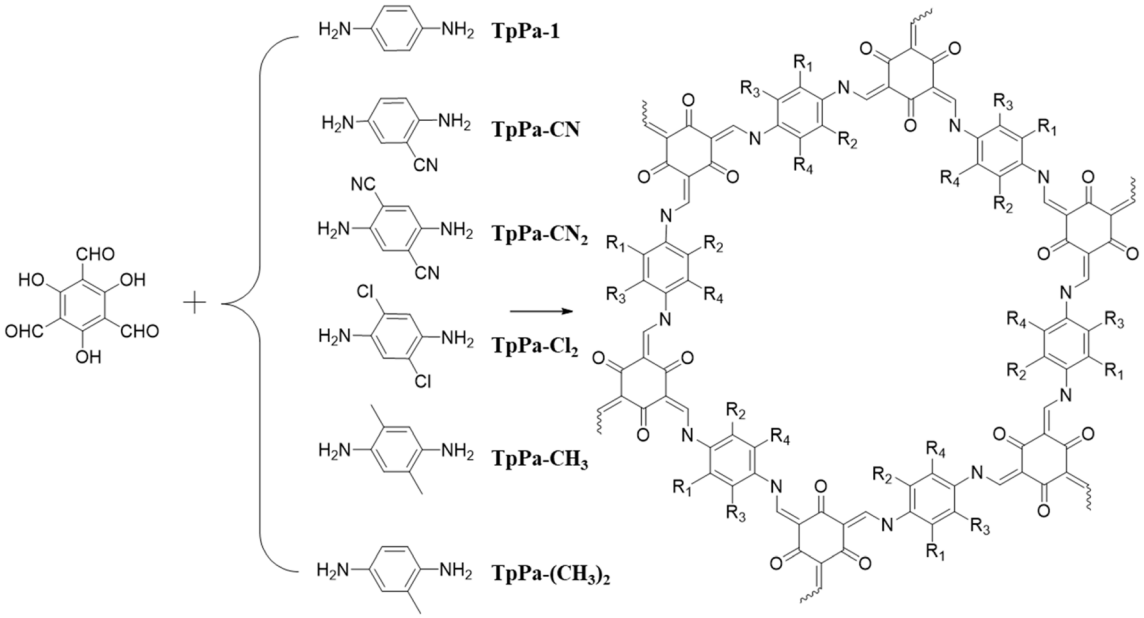

Scheme 1 Bottom-up strategy for the synthesis of TpPa-1, TpPa-CN, TpPa-CN_2, TpPa-Cl_2, TpPa-CH_3, and TpPa-$(CH_3)_2$.

Open Access Article. Published on 05 April 2024. Downloaded on 3/13/2026 3:07:41 PM.
This article is licensed under a Creative Commons Attribution-NonCommercial 3.0 Unported Licence.

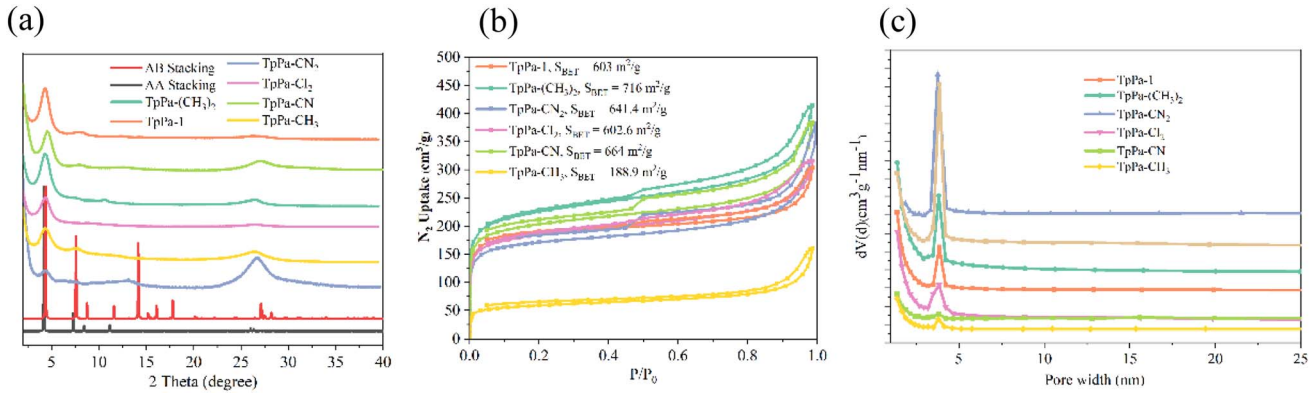

Fig. 1 (a) The powder X-ray diffraction, (b) nitrogen adsorption/desorption isotherms of the six COFs and (c) pore size distributions measured at 77 K for TpPa COFs.

All of the six synthesized COFs showed typical type-IV isotherms, which are characteristic of mesoporous materials. The Brunauer–Emmett–Teller (BET) surface areas of TpPa-Cl_2, TpPa-CN_2, TpPa-CN, TpPa-1, TpPa-$(CH_3)_2$ and TpPa-CH_3 were calculated to be 602, 641, 664, 603, 716 and 188.9 m^2 g^{-1}, with the total pore volumes of 0.467, 0.460, 0.540, 0.425, 0.589 and 0.204 cm^3 g^{-1}, respectively (Fig. 1b). The introduction of substituents in the skeleton did not significantly change the porous structure of these COFs.

The band structure of organic semiconductors plays a crucial role in determining their photoactivity. The UV-visible diffuse reflectance spectra (UV-DRS) analysis revealed that the six different COFs exhibited similar optical absorption capabilities in the visible light range of 400–800 nm. However, when compared to COF-TpPa-1, all the COFs with substituents displayed a slight red shift in the adsorption edge within the range of 500–600 nm (Fig. 2a), suggesting that the introduction of substituents influences the band structure of the COFs, thereby increasing their photoactivity in the visible light region. According to the Tauc plots, the optical band gaps of TpPa-Cl_2, TpPa-CN_2, TpPa-CN, TpPa-1, TpPa-$(CH_3)_2$ and TpPa-CH_3 were calculated to be 2.08, 2.06, 2.07, 2.12, 2.05 and 2.06 eV, respectively (Fig. 2b). The narrowing of the optical band gap proved that the light absorption capacity of these COFs was enhanced. As displayed in Fig. 2c, the flat band potential (E_{FB}) of TpPa-Cl_2, TpPa-CN_2, TpPa-CN, TpPa-1, TpPa-$(CH_3)_2$ and TpPa-CH_3 was determined to be −0.95, −0.86, −0.91, −0,76, −1.01 and −0.85 eV (*vs.* NHE, normal hydrogen electrode), respectively, by extending the linear part of M–S plots. Besides, all the tested samples exhibit a positive slope in M–S plots, indicating the typical n-type semiconductor traits. It is well-known that the conduction band potential (E_{CB}) of n-type semiconductors is typically around 0.2 eV lower than the energy of the Fermi level (E_{FB}). In the case of the COFs studied, the E_{CB} values for TpPa-Cl_2, TpPa-CN_2, TpPa-CN, TpPa-1, TpPa-$(CH_3)_2$ and TpPa-CH_3 were −0.71, −0.62, −0.67, −0.58, −0.77 and −0.61 eV (*vs.* NHE), respectively. According to the equation of $E_{VB} = E_{CB} + E_g$ (E_{VB} is the potential of the valence band (VB)), the E_{VB} of TpPa-Cl_2, TpPa-CN_2, TpPa-CN, TpPa-1, TpPa-$(CH_3)_2$ and TpPa-CH_3 was estimated to be 1.37, 1.43, 0.40, 1.54, 1.28 and 1.45 eV (*vs.* NHE), respectively. Since their E_{CB} values are all more negative than the redox potential of H^+/H_2,[37] all six COFs possess thermodynamically sufficient potentials for the photocatalytic hydrogen evolution reaction (Fig. 2d).

To further investigate the separation efficiency of photogenerated carriers in the six different COFs, transient photocurrent (TPC) and electrochemical impedance measurements were conducted. As shown in Fig. 3a, the introduction of –CN_2, –CN and –Cl_2 in the frameworks enhanced the photocurrent density of COFs under visible light irradiation. The photocurrent density of the TpPa-Cl_2 electrode was almost twice that of the TpPa-1 electrode. In contrast, the photocurrent density of the TpPa-$(CH_3)_2$ and TpPa-CH_3 electrodes was clearly lower than that of the TpPa-1 electrode. The result suggested that the implantation of electron-withdrawing groups can extend the photo-response of COFs to visible light and effectively inhibit the recombination of photogenerated electron–hole pairs, while the electron–donating group can impair the separation efficiency. The electrochemical impedance spectroscopy (EIS) plots demonstrate that the introduction of electron-withdrawing groups into the TpPa-COF does not have a significant impact on the electrochemical impedance. In contrast, when electron-donating groups are incorporated, the electrochemical impedance is noticeably increased. This observation suggests that the presence of electron-donating groups hinders the charge transfer within the COF structure, potentially leading to a decrease in the overall charge transfer efficiency (Fig. 3b).

Furthermore, the transient fluorescence results indicated that the introduction of substituents leads to shorter fluorescence lifetimes (Fig. 3c), in the order of TpPa-1 > TpPa-$(CH_3)_2$ > TpPa-CN_2 > TpPa-CH_3 > TpPa-CN > TpPa-Cl_2, with quantitative determinations of 4.26, 3.10, 2.53, 2.28, 2.18 and 1.98 ns, respectively (Table S2†). This can be attributed to the p–π conjugation generated between the substituents and the full conjugated planes of the COF to enhance the conduction efficiency of the photogenerated carriers.[38–42]

Photocatalytic hydrogen evolution (PHE) experiments were performed under visible light irradiation (λ > 420 nm), using an aqueous solution of ascorbic acid as an electron sacrificial agent and photo-deposition of Pt equivalent to 3 wt% COF from

 This journal is © The Royal Society of Chemistry 2024

Open Access Article. Published on 05 April 2024. Downloaded on 3/13/2026 3:07:41 PM.
This article is licensed under a Creative Commons Attribution-NonCommercial 3.0 Unported Licence.

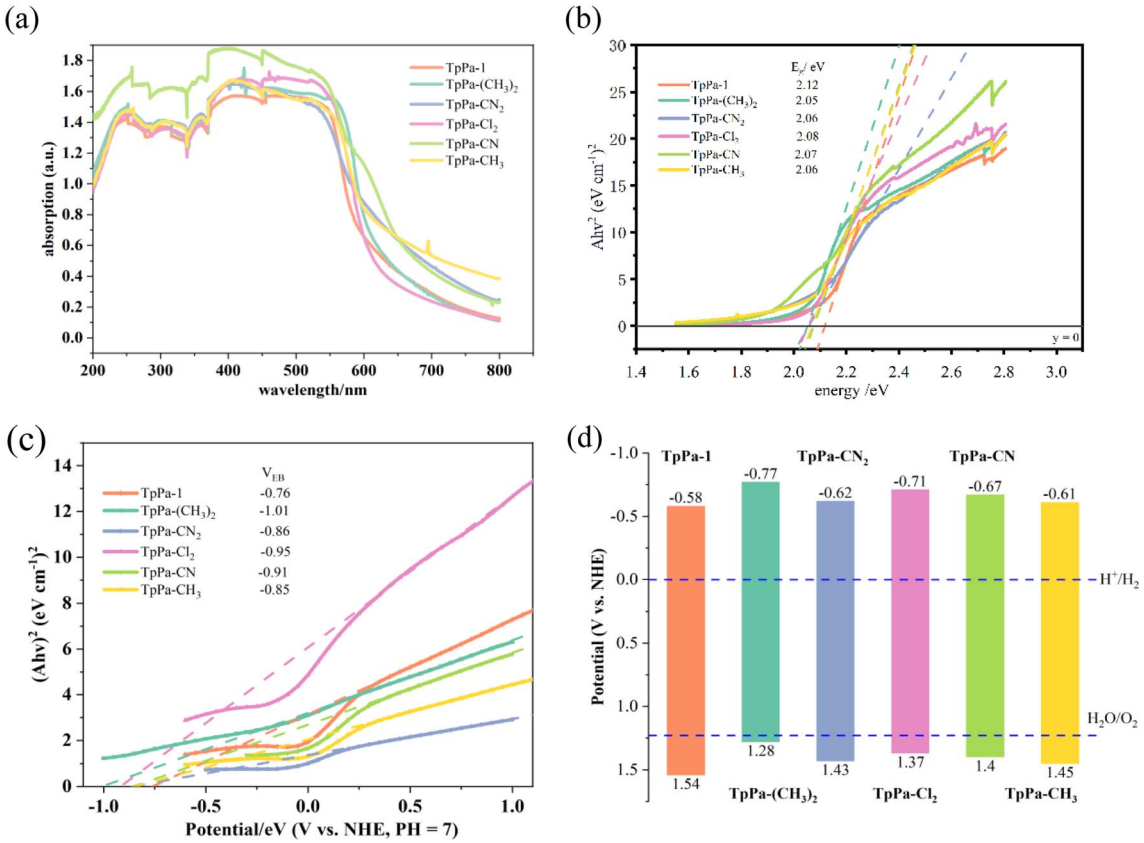

Fig. 2 (a) UV-vis diffuse reflectance spectra, (b) Tauc plots, (c) Mott–Schottky curve and (d) band position of the six COFs.

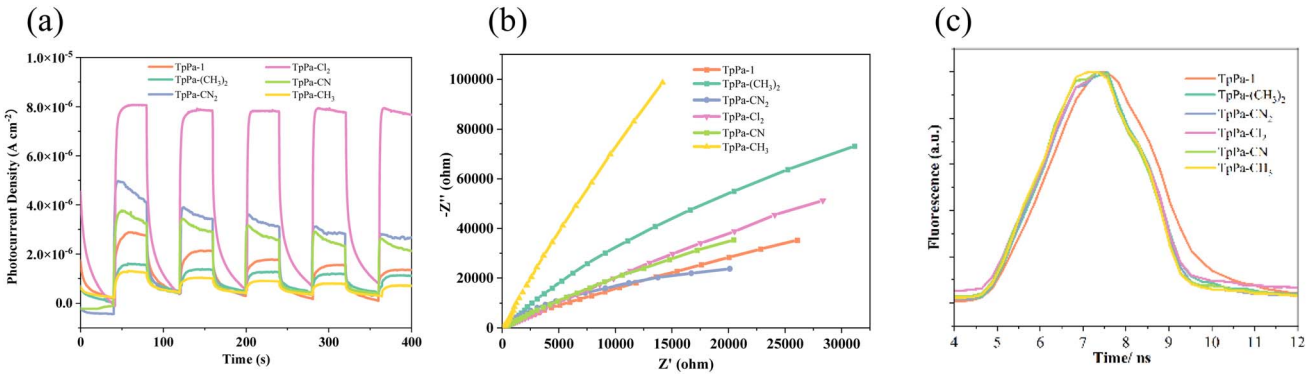

Fig. 3 (a) Transient photocurrent responses, (b) electrochemical impedance spectroscopy and (c) nanosecond-level time-resolved fluorescence decay spectra under 460 nm laser excitation of the six COFs.

hexachloroplatinic acid (H_2PtCl_6) as a cocatalyst. TpPa-Cl_2 showed the highest hydrogen evolution rate, with an average four hour hydrogen evolution rate of 99.226 mmol g^{-1} h^{-1}. The hydrogen evolution rates of the six COFs followed the order of TpPa-Cl_2 (99.23 mmol g^{-1} h^{-1}) > TpPa-CN_2 (76.93 mmol g^{-1} h^{-1}) > TpPa-1 (55.25 mmol g^{-1} h^{-1}) > TpPa-CN (33.01 mmol g^{-1} h^{-1}) > TpPa-$(CH_3)_2$ (25.85 mmol g^{-1} h^{-1}) > TpPa-CH_3 (15.43 mmol g^{-1} h^{-1}) (Fig. 4a). The photocatalytic hydrogen evolution rates of TpPa-Cl_2 and TpPa-CN_2 are higher than those of most of the reported catalysts (Table. S3†). In order to further explore the catalytic performance of the pure COF and to explain the deviation of TpPa-CN catalytic rates, a PHE experiment was performed in the absence of the Pt catalyst. The PHE rates achieved by these COFs were in the order of TpPa-Cl_2 > TpPa-CN_2 > TpPa-CN > TpPa-1 > TpPa-CH_3 > TpPa-$(CH_3)_2$ (Fig. 4b). The PHE ability of COFs without Pt was generally consistent with their TPC order. Obviously, the PHE efficiency of these COFs was exactly related to their photo-responsivity with the exception of TpPa-CN (Fig. 3a). The long-time continuous photocatalytic tests on TpPa-CN_2 and TpPa-Cl_2 showed that

Open Access Article. Published on 05 April 2024. Downloaded on 3/13/2026 3:07:41 PM.
This article is licensed under a Creative Commons Attribution-NonCommercial 3.0 Unported Licence.

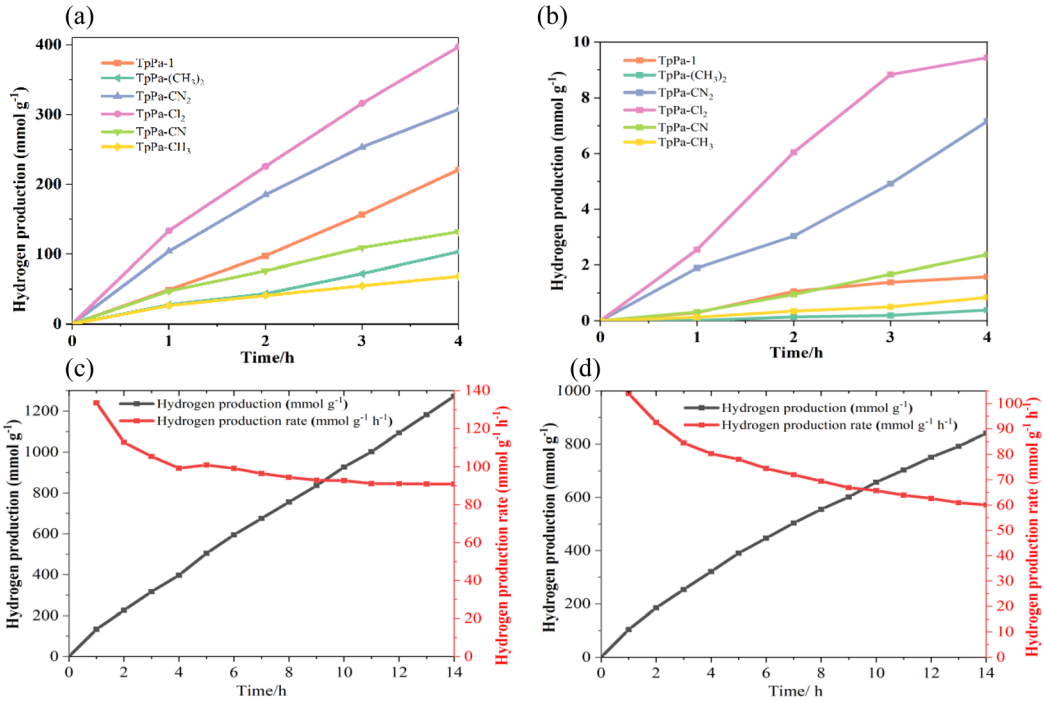

Fig. 4 The PHE rates of the six COFs with (a) and without (b) the Pt NP co-catalyst and PHE rates of TpPa-Cl_2 (c) and TpPa-CN_2 (d) for 14 h in succession.

TpPa-Cl_2 possessed better catalytic stability than TpPa-CN_2 (Fig. 4c and d), which proved that –Cl had a more stable catalytic promotion than –CN. Meanwhile, the XRD patterns of the six COF powders after the PHE reaction proved that all the synthesized COFs had good structural stability (Fig. S2, ESI†).

To further unveil the different behaviors of these COFs with and without Pt NPs in PHE, the morphology and surface chemical states of COFs in the presence and absence of Pt were analyzed using HR-TEM and XPS. Taking TpPa-1 for example, the signals at the binding energy (BE) of 74.03, 284.61, 400.13 and 530.87 eV in the XPS spectrum of TpPa-1/Pt were attributed to Pt, C, N and O elements[43] respectively. The high-resolution Pt 4f XPS spectrum can be deconvoluted into two doublets (Fig. 5b) at 71.6 and 74.6 and 72.5 and 75.8, which can be attributed to the presence of the Pt^0 and Pt^{2+} species, respectively. On the surface of TpPa-Cl_2, TpPa-CN_2 and TpPa-$(CH_3)_2$, the binding energy of Pt^0 $4f_{7/2}$ was shifted to 71.48, 71.20 and 71.53 eV, respectively, which was obviously lower than that on the surface of TpPa-1. This result indicated that the introduction of substituents triggered stronger interaction between Pt NPs and the COF skeleton. In addition, the content of Pt(0) in Pt/COF with –CN and –Cl was obviously higher than that of Pt/TpPa-1, indicating that the Pt/COF with electron-withdrawing substituents could provide more active sites for H_2 evolution. In

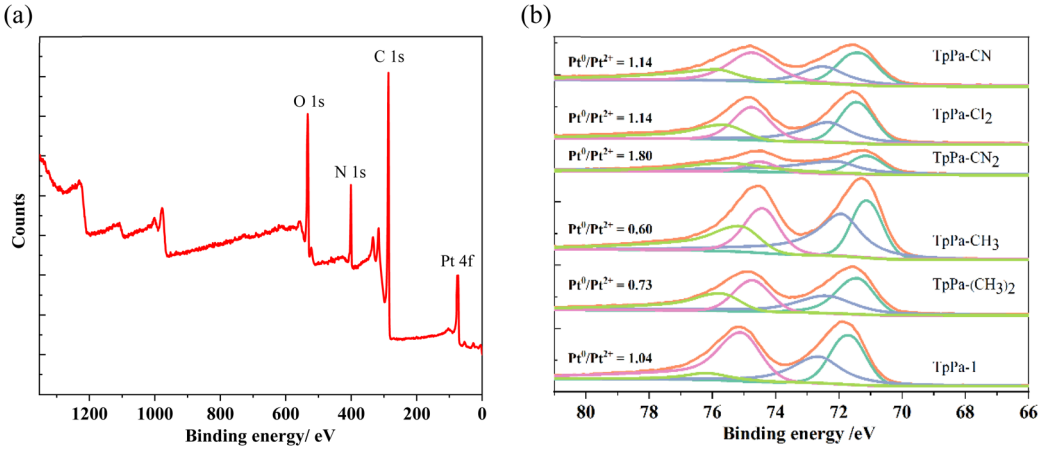

Fig. 5 (a) Full-scan XPS spectrum of TpPa-1/Pt and (b) the high-resolution XPS spectra of Pt 4f on the surface of different COFs.

Open Access Article. Published on 05 April 2024. Downloaded on 3/13/2026 3:07:41 PM.
This article is licensed under a Creative Commons Attribution-NonCommercial 3.0 Unported Licence.

addition, Fig. S3† shows that compared to Pt/TpPa-1, the C 1s binding energy (BE) is blue-shifted and the O 1s BE is red-shifted to a greater extent on the Pt/TpPa-CH_3 surface, while the BE of Pt 4f is significantly lower than that of Pt/TpPa-1, suggesting that the mono CH_3 substituent promotes the movement of electrons towards the amine monomer and Pt. On the surface of Pt/TpPa-$(CH_3)_2$, the BE of each species of C 1s was significantly red-shifted, meanwhile the BEs of O 1s and N 1s moved significantly lower, and the BE of Pt 4f was slightly lower than that of Pt/TpPa-1. This result indicated that the *para*-methyl substituents increased the electron density on the benzene ring, decreased the heterogeneity of the electron distribution on the surface of Pt/TpPa-$(CH_3)_2$, which could reduce the electron transfer between C, O, N, and Pt elements, and was unfavourable for photogenerated electron transfer. For TpPa-CN, the BE shifts of C 1s, N 1s and O 1s before and after loading Pt NPs were similar to those of Pt/TpPa-1, suggesting that mono-cyano substitution did not significantly promote the interaction and electron transfer ability between the COF and Pt. Compared with TpPa-CN_2, the BE of C 1s on the surface of Pt/TpPa-CN_2 was significantly red-shifted and the BE of N 1s was blue-shifted, while the BE of Pt 4f was significantly blue-shifted compared with that of Pt/TpPa-1, indicating that the para-substitution of cyano facilitated the transfer of electrons to the Pt and N atoms and increased the heterogeneity of the electron distribution in favour of the photogenerated carrier separation. For TpPa-Cl_2, the loading of Pt NPs resulted in a blue shift in the BEs of C 1s, N 1s, and O 1s, a red shift in the BE of Cl 2p combined with a blue shift in the BE of Pt 4f compared to Pt/TpPa-1, which suggested the possible electron transfer from the chlorine-substituent to the skeleton of the COF and Pt NPs. In conclusion, $-Cl_2$, and CN_2 promoted the electron transfer ability on the surface of the Pt/TpPa COF system and contributed to the separation of photogenerated carriers.

The morphology of the COFs before and after the PHE reaction was examined using high-resolution transmission electron microscopy (HR-TEM). The HR-TEM images revealed that all six COFs exhibited a similar clustered rod-like morphology (Fig. S4, ESI†). During the PHE process, Pt NPs were uniformly deposited on the surfaces of TpPa-1, TpPa-CH_3 and TpPa-$(CH_3)_2$ COFs. But Pt NPs on the surface of TpPa-Cl_2 and TpPa-CN_2 were larger in diameter and somewhat aggregated compared to those on TpPa-1. This phenomenon can be attributed to the stronger interaction between the electron-withdrawing groups present and the Pt NPs. This interaction causes the Pt NPs to grow into larger particles around the electron-absorbing groups. In the case of TpPa-CN, the density of Pt NPs was relatively low, and the aggregation degree of the Pt NPs was more severe compared to the COF without substituents. The larger particle size and lower loading efficiency of Pt NPs on the surface of TpPa-CN might contribute to its poorer PHE performance than TpPa-1.[44]

The introduction of electron-withdrawing substituents, such as –CN and –Cl, into the skeleton of TpPa COFs improved their hydrophilicity (Fig. S5, ESI†). In contrast, the presence of the electron-donating substituent methyl decreased the hydrophilicity of TpPa COFs. The hydrophilic surface is beneficial for the interaction between the photocatalyst and water, facilitating efficient charge transfer from the photocatalyst to water and ultimately enhancing hydrogen evolution.[45]

3. Conclusion

The above-mentioned results indicated that the implantation of substituents in the skeleton has little effect on the band structure of COFs, but can affect the visible-light response, separation ability of photo-induced carriers, loading of Pt NPs and surface hydrophilicity. The electron-withdrawing substituents are conducive to the improvement of light response of COFs, while the electron-donating groups brought about a negative effect on visible-light absorption and production of photo-carriers. Therefore, the COFs bearing electron-withdrawing groups in the skeleton showed higher PHE efficiency compared to TpPa-1. However, stronger interaction between Pt NPs and substituents in COFs leads to aggregation of Pt NPs on the surface of COFs, which gives rise to decreased PHE rates. Therefore, the PHE ability of COFs can be efficiently tuned just by subtly regulating the types of substituents in the skeleton of monomers.

Data availability

Data available in the ESI: reagents, instrumentation, experimental method, preparation details, HR-TEM and contact angle test.†

Conflicts of interest

There are no conflicts to declare.

Acknowledgements

This work was jointly supported by the National Natural Science Foundation of China (22320102005, 22036007, and 22276207), the National Key Research and Development Program of China (2022YFC3701401) and Jinan University and Institute Innovation Team Project (202228045).

References

1 T. Takata, J. Jiang, Y. Sakata, M. Nakabayashi, N. Shibata, V. Nandal, K. Seki, T. Hisatomi and K. Domen, Photocatalytic water splitting with a quantum efficiency of almost unity, *Nature*, 2020, **581**(7809), 411–414.
2 Y. Yang, N. Luo, S. Lin, H. Yao and Y. Cai, Cyano substituent on the olefin linkage: promoting rather than inhibiting the performance of covalent organic frameworks, *ACS Catal.*, 2022, **12**(17), 10718–10726.
3 A. Bavykina, N. Kolobov, I. S. Khan, J. A. Bau, A. Ramirez and J. Gascon, Metal–organic frameworks in heterogeneous catalysis: recent progress, new trends, and future perspectives, *Chem. Rev.*, 2020, **120**(16), 8468–8535.

Open Access Article. Published on 05 April 2024. Downloaded on 3/13/2026 3:07:41 PM.
This article is licensed under a Creative Commons Attribution-NonCommercial 3.0 Unported Licence.

4 X. Gan, D. Lei and K.-Y. Wong, Two-dimensional layered nanomaterials for visible-light-driven photocatalytic water splitting, *Mater. Today Energy*, 2018, **10**, 352–367.
5 Q. Wang and K. Domen, Particulate photocatalysts for light-driven water splitting: mechanisms, challenges, and design strategies, *Chem. Rev.*, 2020, **120**(2), 919–985.
6 W. Li, A. Elzatahry, D. Aldhayan and D. Zhao, Core–shell structured titanium dioxide nanomaterials for solar energy utilization, *Chem. Soc. Rev.*, 2018, **47**(22), 8203–8237.
7 Y. Wang, A. Vogel, M. Sachs, R. S. Sprick, L. Wilbraham, S. J. A. Moniz, R. Godin, M. A. Zwijnenburg, J. R. Durrant, A. I. Cooper and J. Tang, Current understanding and challenges of solar-driven hydrogen generation using polymeric photocatalysts, *Nat. Energy*, 2019, **4**(9), 746–760.
8 Q. Guo, C. Zhou, Z. Ma and X. Yang, Fundamentals of TiO_2 photocatalysis: concepts, mechanisms, and challenges, *Adv. Mater.*, 2019, **31**(50), 1901997.
9 A. P. Côté, A. I. Benin, N. W. Ockwig, M. O'Keeffe, A. J. Matzger and O. M. Yaghi, Porous, crystalline, covalent organic frameworks, *Science*, 2005, **310**(5751), 1166–1170.
10 L. He, L. Chen, X. Dong, S. Zhang, M. Zhang, X. Dai, X. Liu, P. Lin, K. Li, C. Chen, T. Pan, F. Ma, J. Chen, M. Yuan, Y. Zhang, L. Chen, R. Zhou, Y. Han, Z. Chai and S. Wang, A nitrogen-rich covalent organic framework for simultaneous dynamic capture of iodine and methyl iodide, *Chem*, 2021, **7**(3), 699–714.
11 C. Liu, Y. Jin, Z. Yu, L. Gong, H. Wang, B. Yu, W. Zhang and J. Jiang, Transformation of porous organic cages and covalent organic frameworks with efficient iodine vapor capture performance, *J. Am. Chem. Soc.*, 2022, **144**(27), 12390–12399.
12 J. Li, Y. Yang, W. Ma, G. Li, Q. Lu and Z. Lin, One-pot room-temperature synthesis of covalent organic framework-coated superhydrophobic sponges for highly efficient oil-water separation, *J. Hazard. Mater.*, 2021, **411**, 125190.
13 C. R. DeBlase, K. E. Silberstein, T.-T. Truong, H. D. Abruña and W. R. Dichtel, β-Ketoenamine-linked covalent organic frameworks capable of pseudocapacitive energy storage, *J. Am. Chem. Soc.*, 2013, **135**(45), 16821–16824.
14 Y. Yang, X. He, P. Zhang, Y. H. Andaloussi, H. Zhang, Z. Jiang, Y. Chen, S. Ma, P. Cheng and Z. Zhang, Combined intrinsic and extrinsic proton conduction in robust covalent organic frameworks for hydrogen fuel cell applications, *Angew. Chem., Int. Ed.*, 2020, **59**(9), 3678–3684.
15 L. Stegbauer, K. Schwinghammer and B. V. Lotsch, A hydrazone-based covalent organic framework for photocatalytic hydrogen production, *Chem. Sci.*, 2014, **5**(7), 2789–2793.
16 X. Wang, W. Zhou, H. Wu and W.-Q. Deng, Protocol for fabrication and characterization of Fe-SAC@COF for electrocatalytic oxygen evolution reaction, *STAR Protoc.*, 2022, **3**(3), 101626.
17 X. Wang, X. Han, J. Zhang, X. Wu, Y. Liu and Y. Cui, Homochiral 2D porous covalent organic frameworks for heterogeneous asymmetric catalysis, *J. Am. Chem. Soc.*, 2016, **138**(38), 12332–12335.
18 J. Wang, X. Yang, T. Wei, J. Bao, Q. Zhu and Z. Dai, Fe-porphyrin-based covalent organic framework as a novel peroxidase mimic for a one-pot glucose colorimetric assay, *ACS Appl. Bio Mater.*, 2018, **1**(2), 382–388.
19 S. Dalapati, C. Gu and D. Jiang, Luminescent porous polymers based on aggregation-induced mechanism: design, synthesis and functions, *Small*, 2016, **12**(47), 6513–6527.
20 D. Kaleeswaran, P. Vishnoi and R. Murugavel, [3+3] Imine and β-ketoenamine tethered fluorescent covalent-organic frameworks for CO_2 uptake and nitroaromatic sensing, *J. Mater. Chem. C*, 2015, **3**(27), 7159–7171.
21 J. Mei, N. L. C. Leung, R. T. K. Kwok, J. W. Y. Lam and B. Z. Tang, Aggregation-induced emission: together we shine, united we soar!, *Chem. Rev.*, 2015, **115**(21), 11718–11940.
22 J. Yang, Y. Cao, W. Si, J. Zhang, J. Wang, Y. Qu and W. Qin, Covalent organic frameworks doped with different ratios of OMe/OH as fluorescent and colorimetric sensors, *ChemSusChem*, 2022, **15**(11), e202200100.
23 H. Wang, H. Wang, Z. Wang, L. Tang, G. Zeng, P. Xu, M. Chen, T. Xiong, C. Zhou, X. Li, D. Huang, Y. Zhu, Z. Wang and J. Tang, Covalent organic framework photocatalysts: structures and applications, *Chem. Soc. Rev.*, 2020, **49**(12), 4135–4165.
24 S. Ma, T. Deng, Z. Li, Z. Zhang, J. Jia, Q. Li, G. Wu, H. Xia, S.-W. Yang and X. Liu, Photocatalytic hydrogen production on a sp^2-carbon-linked covalent organic framework, *Angew. Chem., Int. Ed.*, 2022, **61**(42), e202208919.
25 P. Dong, A. Zhang, T. Cheng, J. Pan, J. Song, L. Zhang, R. Guan, X. Xi and J. Zhang, 2D/2D S-scheme heterojunction with a covalent organic framework and g-C_3N_4 nanosheets for highly efficient photocatalytic H_2 evolution, *Chin. J. Catal.*, 2022, **43**(10), 2592–2605.
26 P. Dong, Y. Wang, A. Zhang, T. Cheng, X. Xi and J. Zhang, Platinum single atoms anchored on a covalent organic framework: boosting active sites for photocatalytic hydrogen evolution, *ACS Catal.*, 2021, **11**(21), 13266–13279.
27 V. S. Vyas, F. Haase, L. Stegbauer, G. Savasci, F. Podjaski, C. Ochsenfeld and B. V. Lotsch, A tunable azine covalent organic framework platform for visible light-induced hydrogen generation, *Nat. Commun.*, 2015, **6**(1), 8508.
28 C. Li, J. Liu, H. Li, K. Wu, J. Wang and Q. Yang, Covalent organic frameworks with high quantum efficiency in sacrificial photocatalytic hydrogen evolution, *Nat. Commun.*, 2022, **13**(1), 2357.
29 L. Wang, L. Zhang, B. Lin, Y. Zheng, J. Chen, Y. Zheng, B. Gao, J. Long and Y. Chen, Activation of carbonyl oxygen sites in β-ketoenamine-linked covalent organic frameworks *via* cyano conjugation for efficient photocatalytic hydrogen evolution, *Small*, 2021, **17**(24), 2101017.
30 Z. Mi, T. Zhou, W. Weng, J. Unruangsri, K. Hu, W. Yang, C. Wang, K. A. I. Zhang and J. Guo, Covalent organic frameworks enabling site isolation of viologen-derived electron-transfer mediators for stable photocatalytic hydrogen evolution, *Angew. Chem., Int. Ed.*, 2021, **60**(17), 9642–9649.

 This journal is © The Royal Society of Chemistry 2024

Open Access Article. Published on 05 April 2024. Downloaded on 3/13/2026 3:07:41 PM.
This article is licensed under a Creative Commons Attribution-NonCommercial 3.0 Unported Licence.

31 Y. Guo, Q. Zhou, B. Zhu, C. Y. Tang and Y. Zhu, Advances in organic semiconductors for photocatalytic hydrogen evolution reaction, *EES Catal.*, 2023, **1**(4), 333–352.

32 X. Li, L. Zhang, S. Niu, Z. Dong and C. Lyu, Quantitatively regulating the ketone structure of triazine-based covalent organic frameworks for efficient visible-light photocatalytic degradation of organic pollutants: Tunable performance and mechanisms, *J. Hazard. Mater.*, 2023, **444**, 130366.

33 Q. Liao, Q. Sun, H. Xu, Y. Wang, Y. Xu, Z. Li, J. Hu, D. Wang, H. Li and K. Xi, Regulating relative nitrogen locations of diazine functionalized covalent organic frameworks for overall H_2O_2 photosynthesis, *Angew. Chem., Int. Ed.*, 2023, **62**(41), e202310556.

34 W. Dong, Z. Qin, K. Wang, Y. Xiao, X. Liu, S. Ren and L. Li, Isomeric oligo(phenylenevinylene)-based covalent organic frameworks with different orientation of imine bonds and distinct photocatalytic activities, *Angew. Chem., Int. Ed.*, 2023, **62**(5), e202216073.

35 H. Yang, M. Hao, Y. Xie, X. Liu, Y. Liu, Z. Chen, X. Wang, G. I. N. Waterhouse and S. Ma, Tuning local charge distribution in multicomponent covalent organic frameworks for dramatically enhanced photocatalytic uranium extraction, *Angew. Chem., Int. Ed.*, 2023, **62**(30), e202303129.

36 J. Cheng, Y. Wu, W. Zhang, J. Zhang, L. Wang, M. Zhou, F. Fan, X. Wu and H. Xu, Fully conjugated 2D sp2 carbon-linked covalent organic frameworks for photocatalytic overall water splitting, *Adv. Mater.*, 2024, **36**(6), 2305313.

37 C. Mo, M. Yang, F. Sun, J. Jian, L. Zhong, Z. Fang, J. Feng and D. Yu, Alkene-linked covalent organic frameworks boosting photocatalytic hydrogen evolution by efficient charge separation and transfer in the presence of sacrificial electron donors, *Adv. Sci.*, 2020, **7**(12), 1902988.

38 Z. Zhang, Y. Zhu, X. Chen, H. Zhang and J. Wang, A full-spectrum metal-free porphyrin supramolecular photocatalyst for dual functions of highly efficient hydrogen and oxygen evolution, *Adv. Mater.*, 2019, **31**(7), 1806626.

39 Y. Yang, H. Niu, W. Zhao, L. Xu, H. Zhang and Y. Cai, Ultrafine Pd nanoparticles loaded benzothiazole-linked covalent organic framework for efficient photocatalytic C–C cross-coupling reactions, *RSC Adv.*, 2020, **10**(49), 29402–29407.

40 Y. Yang, H. Niu, L. Xu, H. Zhang and Y. Cai, Triazine functionalized fully conjugated covalent organic framework for efficient photocatalysis, *Appl. Catal., B*, 2020, **269**, 118799.

41 P.-F. Wei, M.-Z. Qi, Z.-P. Wang, S.-Y. Ding, W. Yu, Q. Liu, L.-K. Wang, H.-Z. Wang, W.-K. An and W. Wang, Benzoxazole-linked ultrastable covalent organic frameworks for photocatalysis, *J. Am. Chem. Soc.*, 2018, **140**(13), 4623–4631.

42 C. Gao, H. Yu, L. Zhang, Y. Zhao, J. Xie, C. Li, K. Cui and J. Yu, Ultrasensitive paper-based photoelectrochemical sensing platform enabled by the polar charge carriers-created electric field, *Anal. Chem.*, 2020, **92**(4), 2902–2906.

43 S. Feng, M. Yan, Y. Xue, J. Huang and X. Yang, An electrochemical sensor for sensitive detection of dopamine based on a COF/Pt/MWCNT–COOH nanocomposite, *Chem. Commun.*, 2022, **58**(41), 6092–6095.

44 H. Wang, X.-K. Gu, X. Zheng, H. Pan, J. Zhu, S. Chen, L. Cao, W.-X. Li and J. Lu, Disentangling the size-dependent geometric and electronic effects of palladium nanocatalysts beyond selectivity, *Sci. Adv.*, 2019, **5**(1), eaat6413.

45 K. Lin, Z. Wang, Z. Hu, P. Luo, X. Yang, X. Zhang, M. Rafiq, F. Huang and Y. Cao, Amino-functionalised conjugated porous polymers for improved photocatalytic hydrogen evolution, *J. Mater. Chem. A*, 2019, **7**(32), 19087–19093.